PNAS
www.pnas.org

Supplemental Information:

The role of Ca^{2+} and protein scaffolding in the formation in nature's water oxidizing complex

Anton P. Avramov, Hong J. Hwang, and Robert L. Burnap

Corresponding Author: Robert L. Burnap

E-mail: rob.burnap@okstate.edu

This PDF file includes:

Figures S1 to S12

Tables S1 to S3

SI References

Other supplementary materials for this manuscript include the following:

none

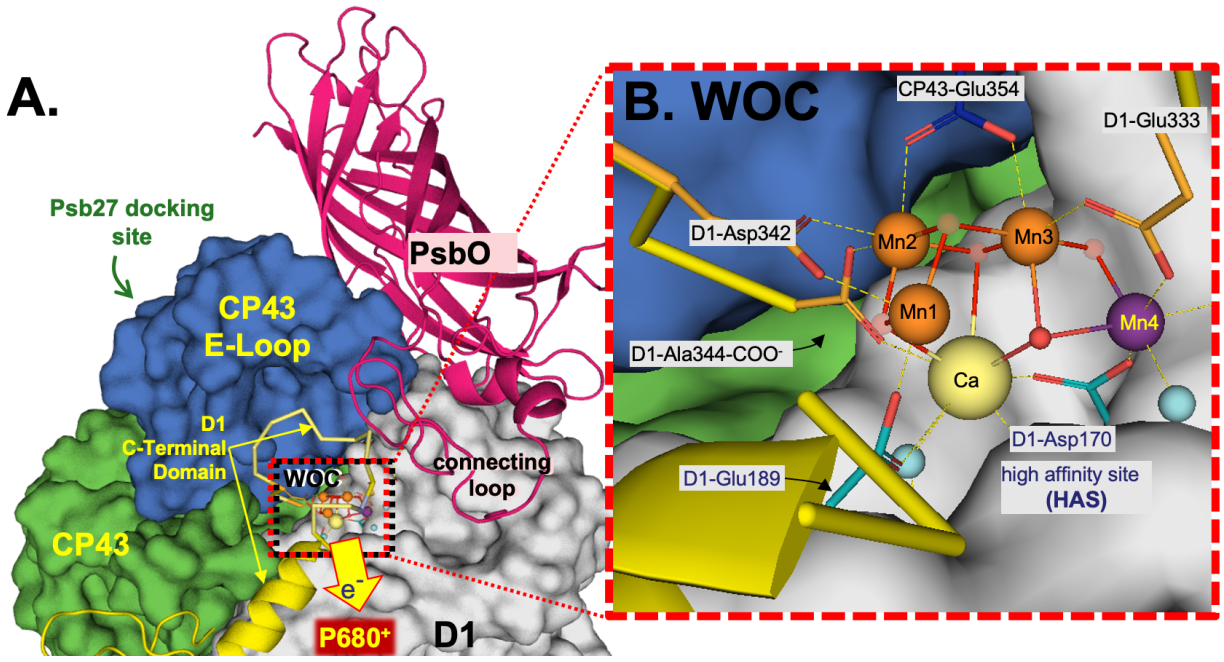

Figure S1. Panel A: The CP43 E-loop **(Blue)** interacts with the metal binding C-terminal domain (**Yellow**), and their coupled mobility controls access to the apo-WOC, modulated by interactions with PsbO and Psb27. **Panel B**: Catalytic Mn_4CaO_5 cluster at the interface between the D1 (PsbA) and CP43 (PsbC) subunits. During photoassembly, Mn^{2+} binds at the high affinity site (**HAS**) at or near the Mn4 (**purple sphere**) involving the D1-Asp170 carboxylate moiety (16, 17), which also ligates Ca^{2+} (**yellow sphere**) at the calcium site (**CAS**). Additional Mn^{2+} ions are photooxidatively incorporated via the oxo-bridges presumably derived from water ligands. A second Mn^{2+} binding site (**SMS**, see text) is critical to trap the first stable intermediate and could include amino acid ligands at one of the other three Mn locations (**orange spheres**). The 'dark' rearrangement, k_D (see Figure 1 main text) is proposed to involve the movement of the E-loop coupled to the D1-carboxyterminal domain which is likely to include the repositioning of the key metal ligands CP43-Glu354, D1-Asp342, and the terminal carboxyl of D1-A344. Psb27 appears to modulate the conformational fluctuations to optimize the repositioning.

Table S1. Photoactivation of hydroxylamine (HA)-extracted and non-extracted membrane samples obtained from *Synechocystis* WT control, Δ*psbO* and *27OE* strains. Photoactivation was produced by application of 1000 saturating single turnover xenon flashes in HA-extracted thylakoid samples containing 40 µg of Chl, which were suspended in 400 µL of in Chelex-100-treated photoactivation buffer in a modified aluminum weight cup with a stirring bar. Maximal rates of oxygen evolution were determined for both HA-extracted and unextracted samples. Aliquots containing 10 µg of chlorophyll were taken and used to measure light saturated oxygen evolution rate at 30 °C using Clark-type electrode in a buffer containing 50 mM MES-NaOH, 25 mM $CaCl_2$, 10 mM NaCl, 1M sucrose pH 6.5, 1mM 2,6 dichloro-*p*-benzoquinone (DCBQ) and 2.5mM potassium ferricyanide $K_3[Fe(CN)_6]$.

Strain	Non-extracted thylakoid membranes, µmol O_2 (mg Chl)$^{-1}$ h^{-1}	Apo-PSII µmol O_2 (mg Chl)$^{-1}$ h^{-1}	Recovered rate µmol O_2 (mg Chl)$^{-1}$ h^{-1}	% recovery
WT	575.6±13.5	12.1±7	224±5.3	38.9 %
27OE	330±24.8	17± 8.4	193.6±8.5	58.4 %
Δ*psbO*	254.6±17.3	5± 3	146.7±20.4	57.6 %

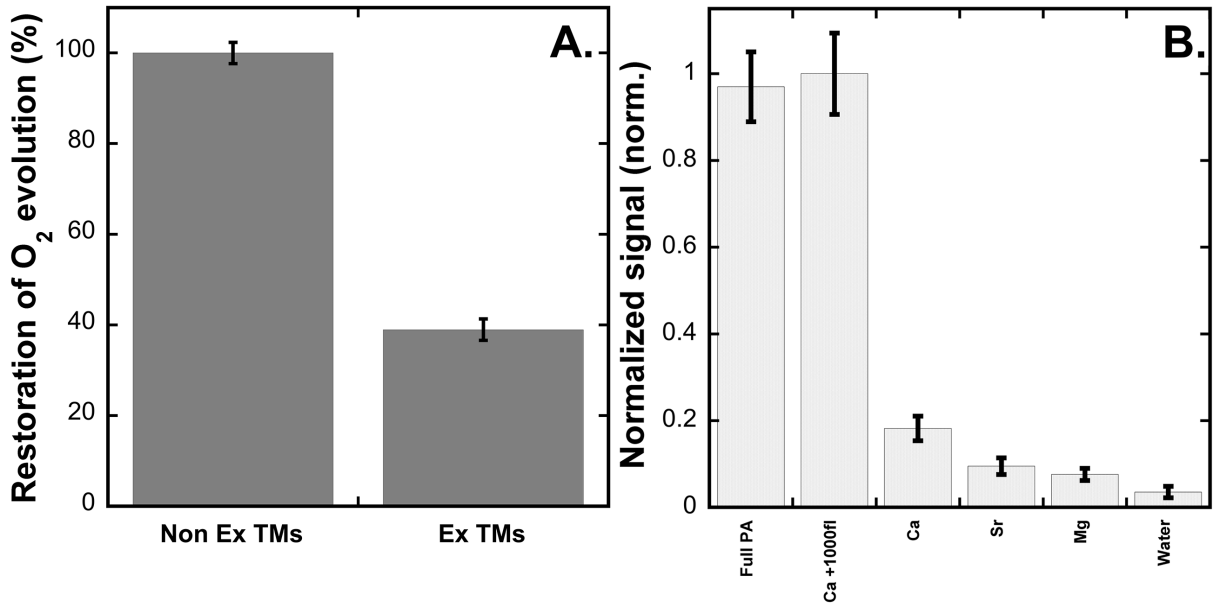

Figure S2. Photoactivation of HA-extracted thylakoid membranes from WT control **Panel A**: Recovery of the light-saturated O_2-evolving activity of hydroxylamine-extracted thylakoid membranes exposed to 15 minutes of continuous illumination. **Panel B**: Effect of post-adding of divalent cations ***after*** illuminating the sample with the sequence of 1000 single turnover flashes at 2Hz (500ms flash interval) in the presence of 250μM $MnCl_2$. The thylakoid membranes were photoactivated using 1000 single-turnover flashes illumination. The 1st photoactivation was carried out in the presence of Mn^{2+} and then cations were added to the photoactivated sample. After incubating for 10 min in the dark on the ice, the photoactivation activity was monitored by measuring O_2 evolution using centrifugal bare platinum electrode using 20 measuring Xenon flashes.

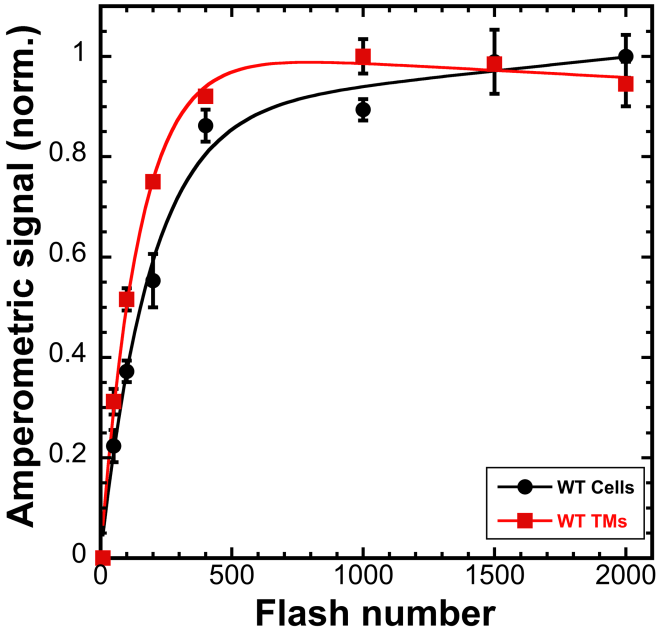

Figure S3. Photoactivation kinetics of hydroxylamine-extracted WT control cells (black circles) and HA-extracted WT control thylakoid membranes (red circles) under sequence of single turnover flashes at 2Hz (500ms flash interval) in the presence of 10mM of $CaCl_2$ and 250μM $MnCl_2$. The photoactivation kinetics of cells and thylakoids were measured on Clark-type electrode and Joliot-type electrode, respectively. Obtained data was fit to $[A]_n = [\mathrm{A}]_0 \cdot (1 - e^{\Phi_{PA} \cdot n}) \cdot (e^{-\Phi_{PI} \cdot n})$ equation (equation 1, see text for details). Error bars represent standard deviation n ≧ 3.

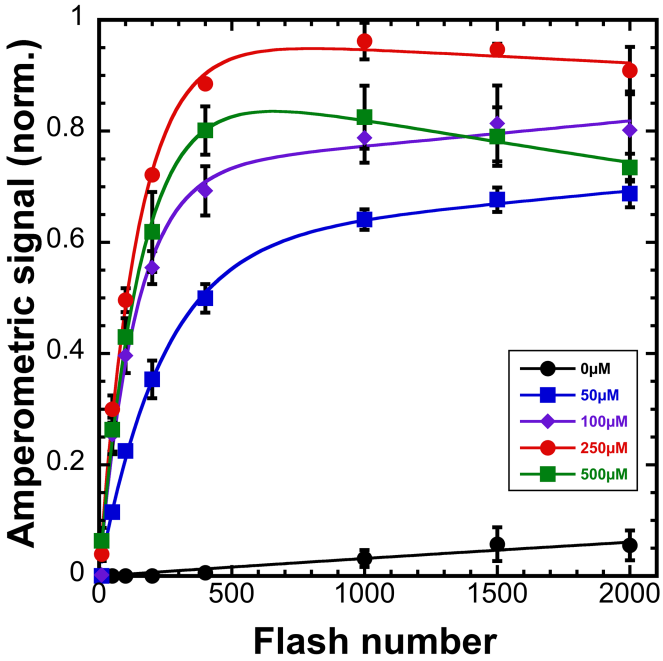

Figure. S4 Manganese dependence of photoactivation under sequence of single turnover flashes at 2Hz (500ms flash interval) of HA-extracted thylakoid membranes from WT control at different Mn^{2+} concentrations: 0μM (black circle), 50μM (blue square), 100μM (purple diamond), 250μM (red circle), and 500μM (green square) of $MnCl_2$ combined with 10mM $CaCl_2$. Data were fit to $[A]_n = [\mathrm{A}]_0 \cdot (1 - e^{\Phi_{PA} \cdot n}) \cdot (e^{-\Phi_{PI} \cdot n})$ equation (equation 1, see text for details). Error bars represent standard deviation n ≧ 3.

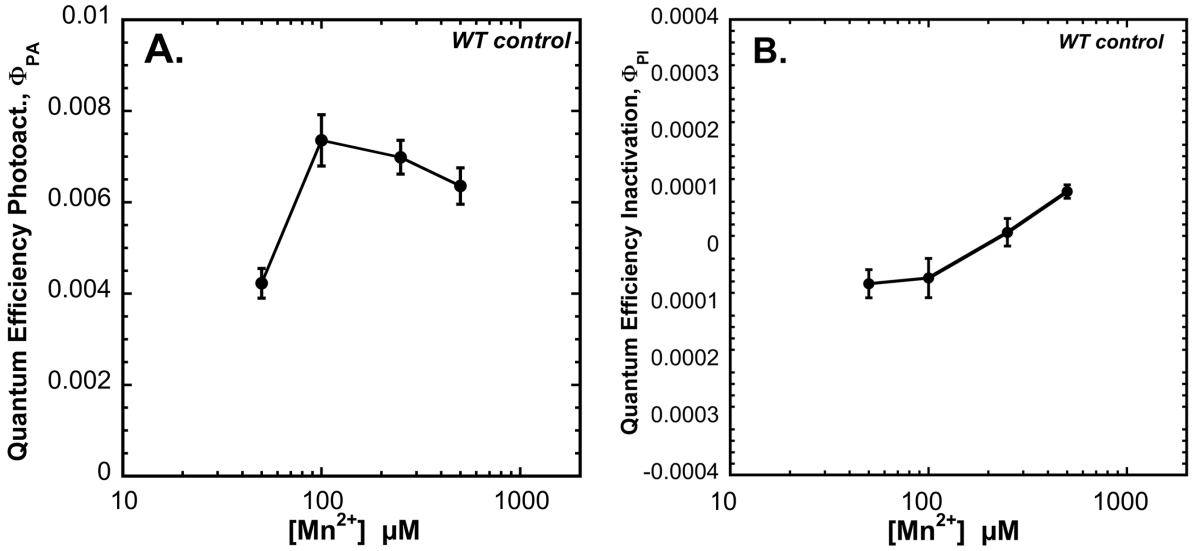

Figure S5. Effect of the different concentrations of $MnCl_2$ at a fixed [Ca^{2+}] = 10 mM on **(A)** Quantum efficiency of photoactivation and **(B)** Quantum efficiency of inactivation in WT control. Kinetic values obtained from fits of data from **Figure S4** to $[A]_n = [\mathrm{A}]_0 \cdot (1 - e^{\Phi_{PA} \cdot n}) \cdot (e^{-\Phi_{PI} \cdot n})$ equation (equation 1, see text for details). Error bars represent standard deviation n ≧ 3.

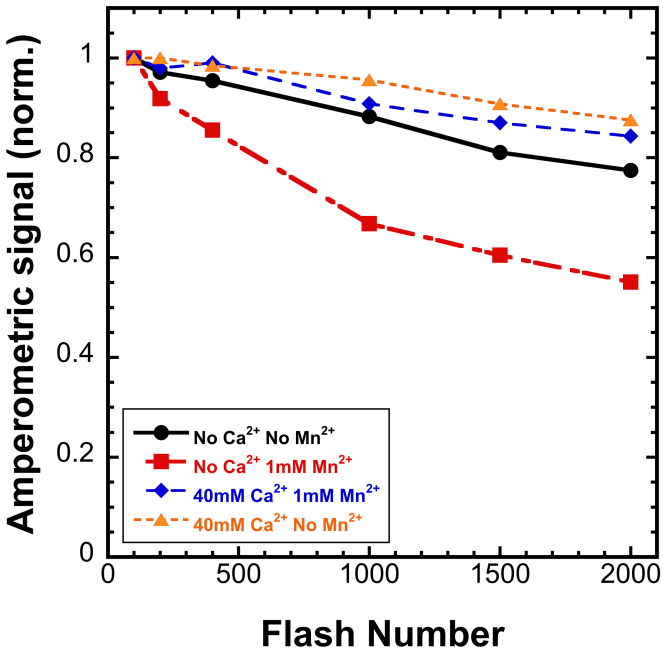

Fig S6. Mn^{2+} induced photoinactivation of oxygen evolution in thylakoid membranes from WT control at different ion availability conditions as a function of the flash number at 2Hz (500ms flash interval) with different amounts of Ca^{2+} and Mn^{2+} added to photoactivation buffer. No Ca^{2+} and no Mn^{2+} (black circles), no Ca^{2+} and 1mM Mn^{2+} (red squares), 40mM Ca2+ and 1mM Mn^{2+} (blue diamond), and 40mM Ca^{2+} and no Mn^{2+} (orange triangles).

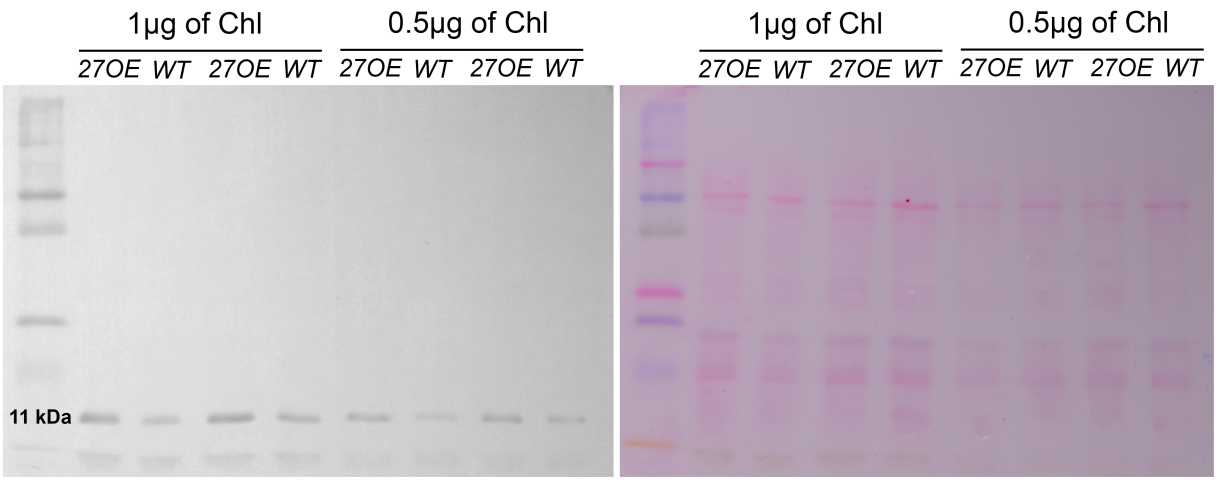

Figure S7. Panel A: Immunological detection of Psb27 expression in WT control expressing normal amount of Psb27 and from *Synechocystis 27OE* mutant over-expressing Psb27 protein. Whole cell extracts samples containing 0.5µg or 1 µg Chl were loaded on a 12% SDS-PAGE gel and transferred to a PVDF membrane. **Panel B**: Prior to immunodetection of Psb27, the same membrane had been stained with 0.5% Ponceau S to verify equal loading. Expression of Psb27 (11kDa) was detected using antibody (a kind gift from Prof. Julian Eaton-Rye, U. Otego, New Zealand). A marker was added for molecular weight comparisons (far-left lane) (Precision Plus Protein Kaleidoscope, Bio-Rad).

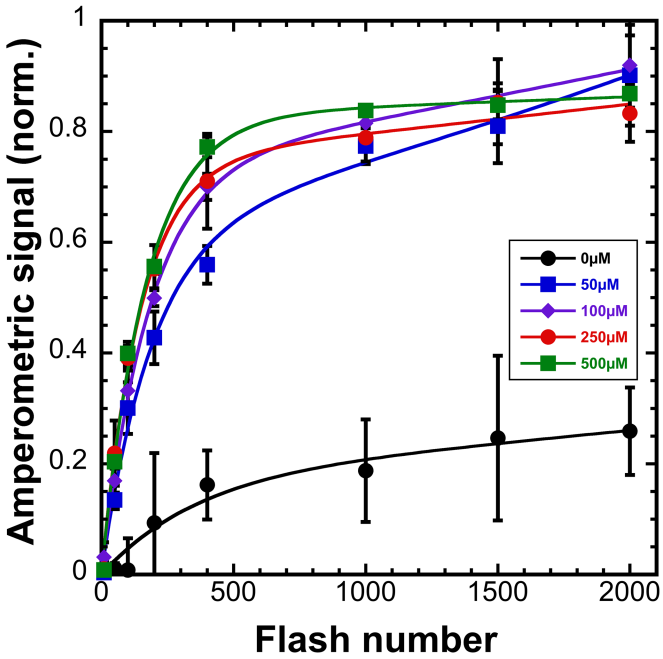

Fig S8. Manganese dependence of photoactivation under sequence of single turnover flashes at 2Hz (500ms flash interval) of HA-extracted thylakoid membranes from ΔpsbO mutant at different Mn^{2+} concentrations: 0µM (black circle), 50µM (blue square), 100µM (purple diamond), 250µM (red circle), and 500µM (green square) of $MnCl_2$ combined with 10mM $CaCl_2$. Data were fit to $[A]_n = [\mathrm{A}]_0 \cdot (1 - e^{\Phi_{PA} \cdot n}) \cdot (e^{-\Phi_{PI} \cdot n})$ equation (Equation 1). Error bars represent standard deviation n ≧ 3.

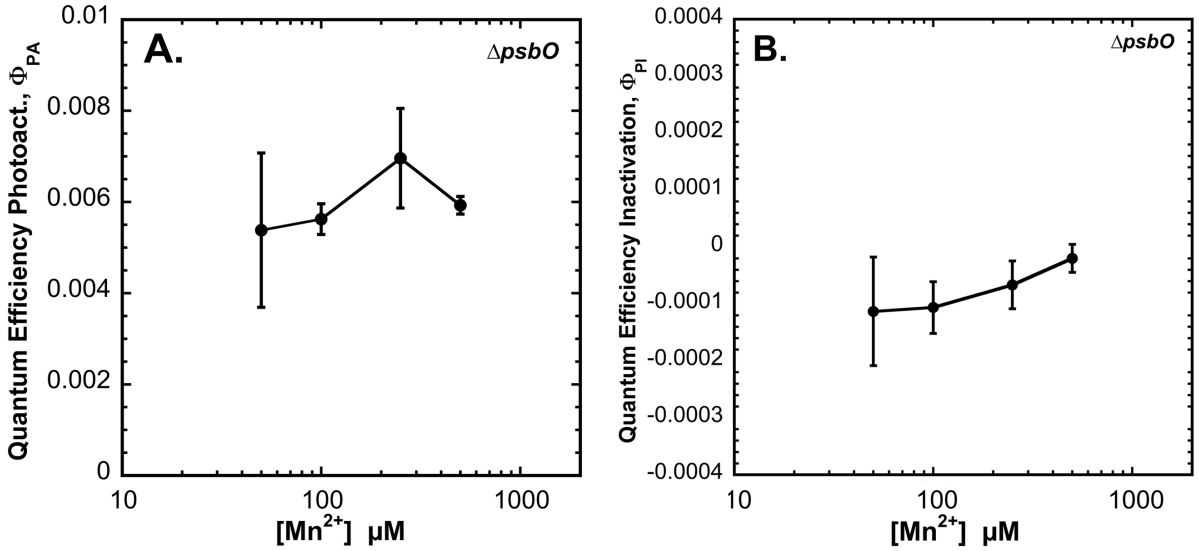

Figure S9. Effect of the different concentrations of $MnCl_2$ at a fixed [Ca^{2+}] = 10 mM on **(A)** Quantum efficiency of photoactivation and **(B)** Quantum efficiency of inactivation in Δ*psbO*. Kinetic values obtained from fits of data from **Figure S8** to $[A]_n = [\mathrm{A}]_0 \cdot (1 - e^{\Phi_{PA} \cdot n}) \cdot (e^{-\Phi_{PI} \cdot n})$ equation (equation 1, see text for details) . Error bars represent standard deviation n ≧ 3.

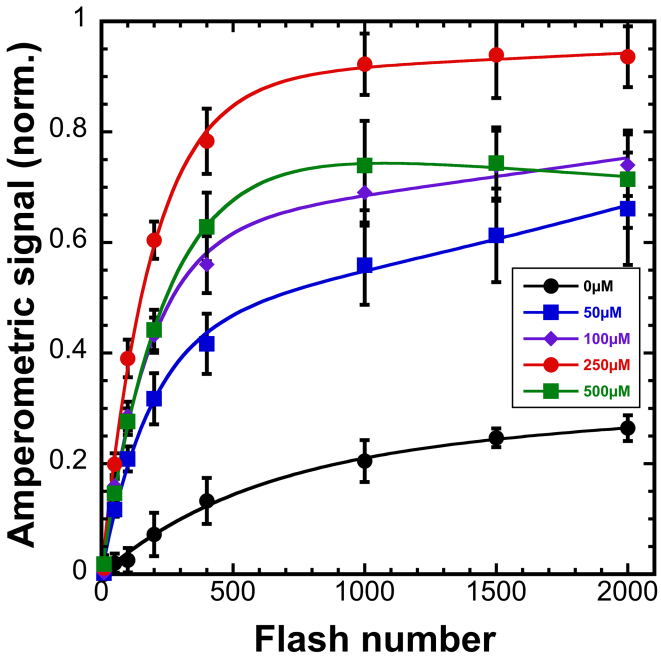

Fig S10 Manganese dependence of photoactivation under sequence of single turnover flashes at 2Hz (500ms flash interval) of HA-extracted thylakoid membranes from 27OE mutant at different Mn^{2+} concentrations: 0μM (black circle), 50μM (blue square), 100μM (purple diamond), 250μM (red circle), and 500μM (green square) combined with 10mM $CaCl_2$. Data were fit to $[A]_n = [\mathrm{A}]_0 \cdot (1 - e^{\Phi_{PA} \cdot n}) \cdot (e^{-\Phi_{PI} \cdot n})$ equation (equation 1, see text for details). Error bars represent standard deviation n ≧ 3.

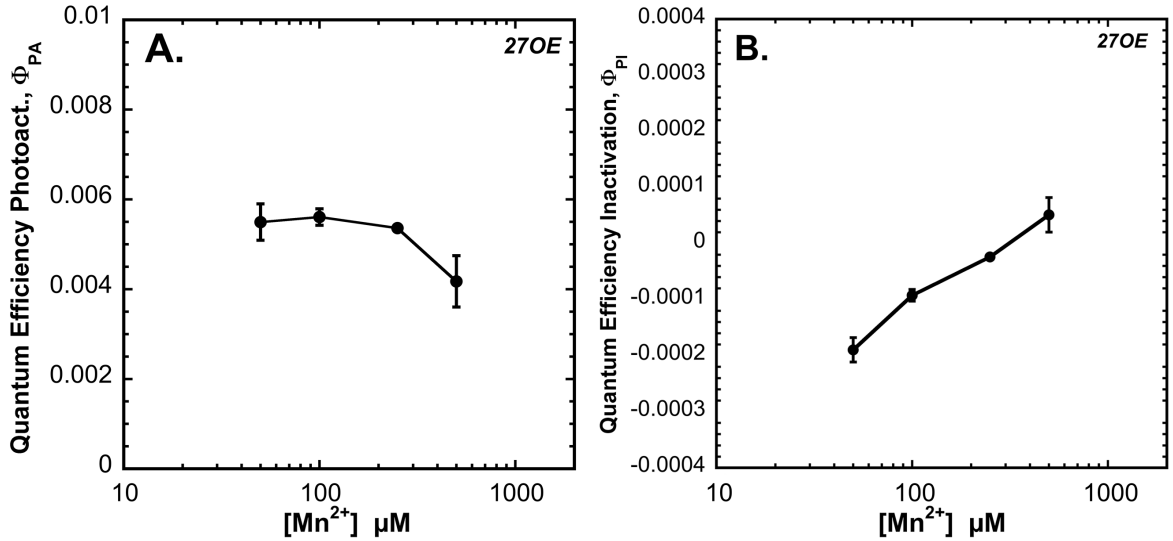

Fig S11. Effect of the different concentrations of $MnCl_2$ at a fixed $[Ca^{2+}]$ = 10 mM on **(A)** Quantum efficiency of photoactivation and **(B)** Quantum efficiency of inactivation in *27OE*. Kinetic values obtained from fits of data from **Figure S10** to $[A]_n = [\mathrm{A}]_0 \cdot (1 - e^{\Phi_{PA} \cdot n}) \cdot (e^{-\Phi_{PI} \cdot n})$ equation (equation 1, see text for details). Error bars represent standard deviation n ≧ 3.

Table S2: DNA Primers used for the cloning and overexpression of the psb27 gene.

Primer name	Sequence
Psb27_GA_F	TACATAAGGAATTATAACCAATGTCCTTTTTGAAAAATCAGTTGTCACGGC
Psb27_GA_R	TTATCAGACCGCTTCTGCGCTCACACGCCCCGTTCAATG
slr1169_seq_F	CGATGATGGCGATCGCCAAAAC
Sp_cassette_seq_R	GGTGGTAACGGCGCAGTG
slr_1285_seq_R	CACCCCCACGCCATCAA
Psb27_seq_F	CCACCGGCATCACCTTTGC

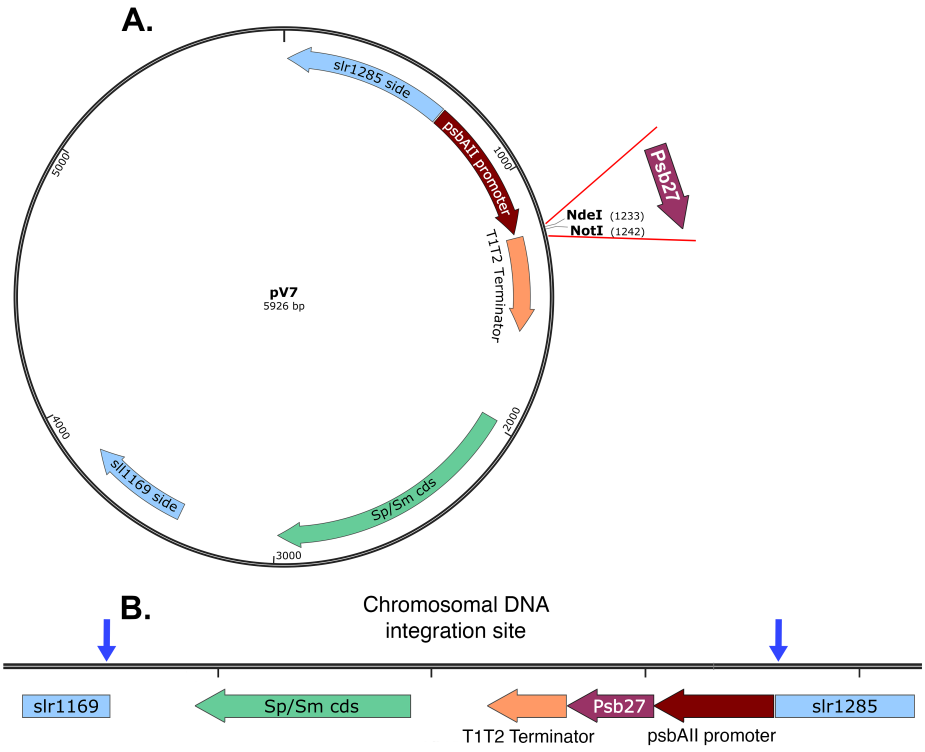

Figure S12. The construction of ectopic expression mutant *27OE*. (A) pV7 plasmid used for the mutant construction, (B) integration of Psb27 gene to the *Synechocystis sp. PCC6803* genome. Arrows indicate the insertion of Psb27 gene with psbAII promoter and T1T2 terminator in conjunction with Spectinomycin/Streptomycin antibiotic resistance cassette. The chromosomal locus comprising the open reading frame slr1645 (Psb27) was amplified by PCR **(Table S2)** using Herculase II Phusion DNA polymerase (Agilent USA). The amplified DNA fragment was assembled into pV7 plasmid (a gift from Hong Wang and Wim Vermaas, Arizona State University) between NotI and NdeI restriction sites using the Gibson Assembly technique (38). The pV7 vector is a suicide plasmid that contains DNA sequences that mediate homologous recombination within the *Synechocystis* chromosome and is designed for the introduction of ectopic overexpression cassettes, in this case, the *psb27* gene was placed under the control of the strong *psbAII* promoter. Transformation results in the integration of the expression cassette at a neutral site within the *Synechocystis* genome between ORFs slr1169 and slr1285.

SI Materials and Methods

At the completion of the photoactivation flash treatment on the bare platinum electrode, flash O_2 yields were recorded as described previously (1-3). The flash O_2 yields were measured using a circuit (4) that sets the polarization of the electrode and amplifies the amperomeric signal due to the appearance of oxygen at the electrode surface during a sequence of saturating single turnover xenon flashes. The relative concentration of photoactivated centers was estimated as the peak height of the oxygen signal recorded after each flash. For the purpose of the Mn^{2+} and Ca^{2+} dependence experiments the values from 50th, 100th, 200th, 400th, 1000th, 1500th and 2000th flashes were used for the data plot generation. At least three replicates for each experiment were obtained. The corresponding peak heights were averaged along with their respective standard deviations. For the experiments measuring photoactivation as a function of flash number, data were normalized to the maximal value obtained within a given dataset corresponding to the entire family of curves shown in that single graph (e.g. **Fig. 2 panel A**). Standard deviation represents normalized standard deviation. In this way, the curves scale, approximately, to the maximal level of photoactivation possible for a given cyanobacterial strain. To analyze the photoactivation kinetics as a function of flash number, data were subjected to various fits starting with the original analysis by G.M. Cheniae and I.F Martin (5), which can be expressed as $[A]_n = [\mathrm{A}]_0 \cdot (1 - e^{\Phi_{PA} \cdot n})$. This original equation describes homogeneous apparent first-order kinetics, where a progressively smaller pool of apo-centers is being photoactivated during the flash sequence as more centers acquire the ability to evolve O_2. Here, $[A]_n$ represents the yield of active centers on the *n*th flash, whereas $[A]_0$, is the concentration of apo-PSII centers prior to the photoactivation, Φ_{PA}, represents the overall efficiency of the multiphoton assembly process. However, to account for the O_2 signal decline due to photoinactivation (6), as second term diminishing the size of the pool of PSII centers was required to describe the data. Several variations, all describing homogeneous quantum efficiency of damage were empirically tested on a range of the data collected, but only one, $[A]_n = [\mathrm{A}]_0 \cdot (1 - e^{\Phi_{PA} \cdot n}) \cdot (e^{-\Phi_{PI} \cdot n})$, where photoinactivation term is represented by $-\Phi_{PI}$, consistently provided reasonable fits (**Table S3**).

Table S3. Equations used for curve fitting of the data obtained from Mn^{2+} and Ca^{2+} dependence as a function of the flash number experiments.

Equation	Notes
$\boldsymbol{[A]_n = [\mathrm{A}]_0 \cdot (1 - e^{\Phi_{PA} \cdot n}) \cdot (e^{-\Phi_{PI} \cdot n})}$ **(*)**	R < 0.995-0.999
$\boldsymbol{[A]_n = [\mathrm{A}]_0 \cdot (1 - e^{\Phi_{PA} \cdot n}) - [\mathrm{A}]_1 (e^{\Phi_{PI} \cdot n})}$	Failed to consistently capture signal decline
$\boldsymbol{[A]_n = [\mathrm{A}]_0 \cdot (1 - e^{\Phi_{PA} \cdot n}) - [\mathrm{A}]_0 (e^{\Phi_{PI} \cdot n})}$	Failed to consistently capture signal decline
$\boldsymbol{[A]_n = [\mathrm{A}]_0 \cdot (1 - e^{\Phi_{PA} \cdot n}) - (e^{\Phi_{PI} \cdot n})}$	Failed to consistently capture signal decline

**Equation used in current study*

To obtain the values for the frequency dependent photoactivation at different $[Ca^{2+}]$, the sample was subjected to 150 single turnover flashes given at different flash intervals. The values from the last six oxygen release peaks were averaged and used in further analysis. Normalization was similar to that described above, but all values shown in a given graph (**e.g. Fig. 3**), were normalized to the maximal averaged data point in that dataset. Estimations of the parameters

under each condition **(Table 1)** describing the dark rearrangement, k_A, and the decay of intermediates, k_D, were determined by deriving kinetic parameters from the rising and falling slopes of the bell-shaped curve in plots of photoactivation as a function of the flash interval curve fitted to the equation (2) originally was derived by Noriaki Tamura and George Cheniae (7) and later used by Hwang et al. (8):

$$[A]_n = [k_A/k_D - k_A] \times [A]_O \times \left(e^{-k_A td} - e^{-k_D td}\right)$$

Photoactivation was also monitored based upon light-saturated steady-state rates of O_2 evolution of the photoactivated thylakoid membranes, using a Clark-type electrode (1, 5, 6). HA-extracted thylakoid samples containing 40 µg of Chl were suspended in 400 µL of in Chelex-100-treated photoactivation buffer in a modified aluminum weight cup with a stirring bar. A series of single-turnover xenon flashes was given to the stirring thylakoid suspension and O_2 evolution rates were in O_2 evolution buffer (50 mM MES-NaOH, 25 mM $CaCl_2$, 10 mM NaCl, and 1M sucrose pH 6.5) at a light intensity of approximately 2500 $\mu Em^{-2}\ s^{-1}$ in the presence of 1mM 2,6 dichloro-*p*-benzoquinone (DCBQ) and 2.5mM potassium ferricyanide $K_3[Fe(CN)_6]$.

SDS-PAGE and Immunoblot analysis. Membrane samples obtained as above were solubilized by addition of 2% SDS, 5mM dithiothreitol, heated at 65 °C for 10 min, and separated on SDS-PAGE (12%). Protein content was transferred to a PVDF membrane using a Bio-Rad (USA) semi-dry apparatus, and membrane was stained with 0.5 % Ponceau S (Sigma) to verify equal loading. 5% BSA solution was used as a blocking agent. Blots were probed against Psb27 (1:750 dilution, a kind gift from Julian Eaton-Rye) with anti-rabbit HRP-conjugated goat antibody (1:3000, Bio-Rad) as a secondary antibody. Color Development was obtained using the chromogenic substrate 4-chloro-1-naphthol (4CN, Bio-Rad) and H_2O_2.

SI References

1. R. L. Burnap, M. Qian, C. Pierce, The manganese-stabilizing protein (MSP) of photosystem II modifies the in vivo deactivation and photoactivation kinetics of the H2O-oxidation complex in Synechocystis sp. PCC6803. *Biochemistry* **35**, 874-882 (1996).
2. H. J. Hwang, A. McLain, R. J. Debus, R. L. Burnap, Photoassembly of the manganese cluster in mutants perturbed in the high affinity Mn-binding site of the H2O-oxidation complex of photosystem II. *Biochemistry* **46**, 13648-13657 (2007).
3. H. Bao, R. L. Burnap, Structural rearrangements preceding dioxygen formation by the water oxidation complex of photosystem II. *Proceedings of the National Academy of Sciences of the United States of America* **112**, E6139-6147 (2015).
4. P. C. Meunier, R. Popovic, High-accuracy oxygen polarograph for photosynthetic systems. *Rev. Sci. Instrum.* **59**, 486-491 (1988).
5. G. M. Cheniae, I. F. Martin, Photoactivation of the manganese catalyst of O_2 evolution. I. Biochemical and kinetic aspects. *Biochimica et biophysica acta* **253**, 167-181 (1971).
6. A. F. Miller, G. W. Brudvig, Manganese and calcium requirements for reconstitution of oxygen evolution activity in manganese-depleted photosystem II membranes. *Biochemistry* **28**, 8181-8190 (1989).
7. N. Tamura, G. Cheniae, Photoactivation of the water-oxidizing complex in Photosystem-II membranes depleted of Mn and extrinsic proteins .1. Biochemical and kinetic characterization. *Biochimica et biophysica acta* **890**, 179-194 (1987).
8. H. J. Hwang, A. McLain, R. J. Debus, R. L. Bumap, Photoassembly of the manganese cluster in mutants perturbed in the high affinity Mn-binding site of the H2O-oxidation complex of photosystem II. *Biochemistry* **46**, 13648-13657 (2007).